The simulation of oscillating wave surge converters using a Boussinesq model; Wave disturbances around an array

Charles E. B. Greenwood, David Christie
Lews Castle College, University of the Highlands and Islands.
Stornoway, Isle of Lewis, Scotland

ABSTRACT

A new method for simulating a frequency independent absorption within DHI's Mike 21 Boussinesq wave (BW) model is presented. This provides an increase in the accuracy of the simulation of wave processes around a hypothetical WEC array. Multiple monochromatic wave simulations are combined to represent a wave spectrum. Wave device characteristics are then simulated using porosity layers. A frequency dependent porosity for each device is then applied based on data taken from an experimental study. This method is tested for nearshore shallow water devices where the wave energy disturbance is quantified for flat and varying domain gradients.

KEY WORDS: Boussinesq wave model, Wave energy modelling, Frequency dependent absorption, Wave-device interactions, Coastal impacts

INTRODUCTION

Over recent years, interest in environmental impacts has driven a more sophisticated treatment of WECs within numerical wave models. Considering individual devices within arrays, rather than solid blocks, has led to a more accurate and detailed description of their effect on the wave climate (Venugopal, Smith 2007, Smith, Pearce & Millar 2012, Greenwood et al. 2013).

Popular simulation methods are reviewed in (Folley *et al.* 2012). Wave resource models conducted using spectral wave software, which provide good representation of wave propagation in coastal waters but lack accurate diffraction terms, should be supplemented by other simulation types to gather more information around wave-device disturbances. The use of Boussinesq/Mild slope models provides a much higher temporal and spatial detail without applying stringent domain size restraints as seen with CFD. Boussinesq models also include an explicit numerical representation of diffraction, allowing an improved simulation behind structures when compare to a spectral wave model.

Boussinesq models have been applied to the simulation of many device types in shallow water environments. Solid open walled structures have been used to simulate the presence of oscillating water columns within the BW model (Venugopal, Bryden & Wallace 2010). While allowing no transmission of energy, the method provides a reasonable approximation for nearshore solid structures. The use of a solid structure is less justifiable to simulate floating or energy permeable structures. Large floating Wave Dragon devices were simulated using a partial transmission of wave energy through a combination of porosity and sponge layers (Torch P. *et al.* 2010, Beels *et al.* 2010). The arms were considered to be permeable, while a sponge layer prevented the transfer of energy through the main body. The detailed analysis of the down-wave results agreed well with experimental data, but largely neglected up-wave effects. In this case, a frequency-independent treatment was justified due to the 0% energy transmission through the body of the device.

Non-terminal devices can be simulated using porosity structures within a BW model. The up and down wave disturbance from a floating hinge type absorber was considered by (Angelelli, Zanuttigh 2012, Angelelli, Zanuttigh & Kofoed 2012). Reasonable agreement with experimental datasets led to the conclusion that a properly calibrated porosity layer provides a good representation of reflected and transmitted waves around a device.

While previous methods have shown reasonable results in simulating specific WECs, device absorption has generally been assumed to be independent of frequency. This study presents a method where a device's frequency response is included. This is conducted for a small array, and the spatial variation of wave disturbance is analysed in detail.

METHODOLGY

The simulation of the propagation of waves was conducted in DHI's MIKE 21 BW (DHI 2012). This software simulates the 2-dimensional propagating waves in shallow water based on Boussinesq formulations (Madsen, Sorensen 1992). The BW model has primarily been used for the simulation of waves of around coastal structures such as harbours and breakwaters. A flap-like nearshore OWSC (Oscillating Wave Surge Converter) was chosen as a frequency-dependent case study. To quantify the change in wave energy around the devices each test case requires two complete models where the undisturbed and the wave-device interactions are simulated. The results of this model are then compared for each element, quantifying the relative change across the whole of the domain.

Frequency Dependent Absorption

Porous structures have been shown to offer a reasonable representation of an energy permeable device. This provides a broad bandwidth of absorption over all frequencies. To better represent an operational device within the BW model a basic frequency dependant absorption can be applied. This uses frequency dependent porosity structures for device simulations, where monochromatic boundary conditions are used. This is achieved by breaking down the incident wave spectrum into frequency bins. Each frequency bin is associated with a monochromatic wave with the same frequency, and amplitude chosen so that the wave's energy is equal to the energy within the bin. Each monochromatic wave is propagated through the model separately, with the absorption altered to match the device's frequency response. The transmitted spectrum is ultimately obtained by combining these monochromatic components. Note that the amplitudes of the individual waves depend on the frequency discretisation, which should be carefully considered to ensure that the individual waves are handled realistically by the BW model.

An experimental frequency based power capture, obtained by (Clabby *et al.* 2012) using a 1:20 scale Aquamarine Power Oyster device for 40 sea states, was adapted to provide a suitable representation of an OWSC. Fig. 1 shows the average frequency dependent power capture for the experimental tests. The power capture, originally normalised on the y-axis, has been de-normalised to adhere to a peak value of 0.2, deemed to be an appropriate peak absorption. A smoothed version of the power capture curve is plotted that reduces variance for higher frequency regions. The frequency dependant absorption was separated into 15 frequency intervals, ranging from 0.06Hz to 0.25Hz with a Δf of 0.01333Hz. The location of each frequency bin is indicated in Fig. 1, where the C_p (power capture) coefficient is indicated. The porosity value for each frequency interval was then given by 1-C_p. This relationship was based on pre-experimental trials where the porosity structure dimensions and behaviour with respect to the incident wave conditions were tested.

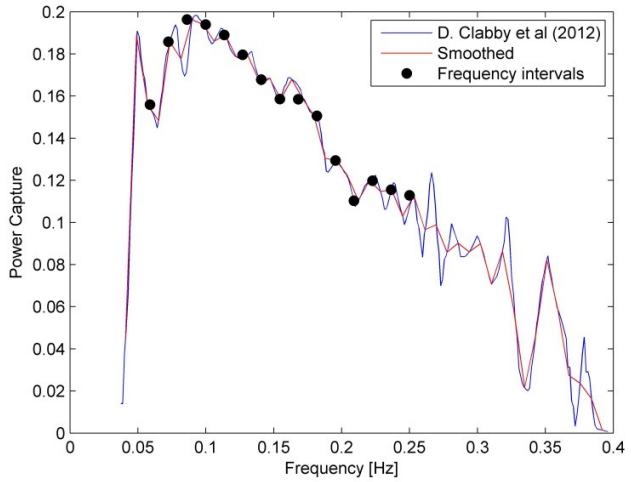

Fig. 1 De-normalized frequency dependent power capture coefficient based on experimental data. 15 frequency intervals have been plotted on the smoothed experimental data.

Model Set-up

The two-dimensional (2D) wave model algorithm was applied to a hypothetical domain with a constant depth of 10m. A 2m regular grid resolution was combined with a time step of 0.15s to produce a Courant number of 0.743. The domain covers an area of 700 x 750 cells (1400m x 1500m). The simulations were run for a time period of 1800s. An internal wave generation line wave used as the driving boundary. The wave conditions were based on a JONSWAP spectrum with an H_s = 2m and T = 10s with the following parameters γ=3.3, σ_a=0.07 and σ_b=0.09. A sponge layer 50 cells thick was applied at either end of the domain to prevent internal wave reflections. Wave breaking and eddy viscosity were enabled where the where the type of roller celerity was set to type 1 and all other terms were kept at their default values.

A small array was positioned at x = 300 cells with an initial device spacing of 100m. The hypothetical device porosity structures use the porosity values listed in Table 1.

Reflected and Transmitted Spectra

To assess the device performance the reflected and transmitted spectra were calculated.

Table 1 Porosity values for an OWSC with regard to frequency.

Frequency	Porosity
0.060	0.844
0.073	0.814
0.087	0.804
1.000	0.806
0.113	0.811
0.127	0.820
0.140	0.832
0.153	0.841
0.167	0.841
0.180	0.879
0.193	0.871
0.207	0.890
0.220	0.880
0.233	0.884
0.247	0.887

The reflected spectrum was calculated using a two wave gauge approach as defined in (Goda, Suzuki 1976). The use of multiple wave height measurements with a separation of 40m was used to calculate K_R (reflection coefficient) at each frequency interval. The frequency varying K_R (shown in Fig. 2) yields a similar distribution to that presented in Fig. 1, where a peak K_R value of above 0.11 occurs at 0.1Hz. At higher frequencies (>0.2Hz) an increase in reflection is depicted, which may be a result of the wave gauge separation nearing the recommended limit stated in (Goda 1985). The data from the reflected spectrum shows increased device reflection at the peak frequency.

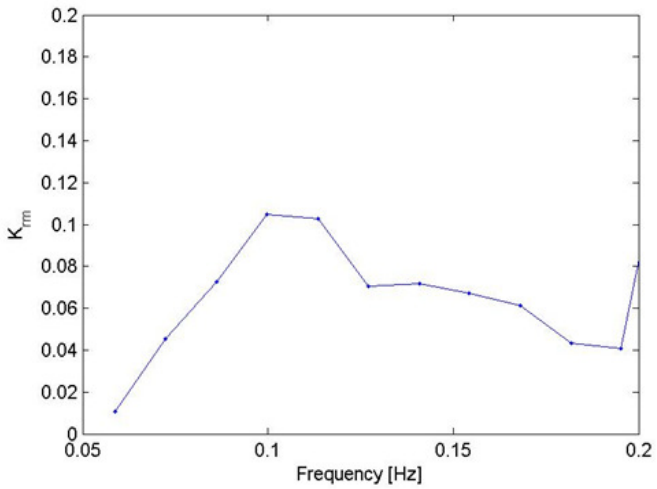

Fig. 2 Frequency dependent reflection coefficients of a hypothetical OWSC.

The transmitted wave spectrum was calculated by using standard linear wave theory to convert the outputted wave heights behind the porosity device to equivalent energies and hence power spectral densities. The results are shown in Fig. 3, where the undisturbed and transmitted wave spectrum indicates a large reduction around the high power capture frequencies (see Fig. 1). The reduction of 5.9m^2/Hz at the 0.1Hz spectral peak represents greatest proportion of wave energy absorption. . As the frequency moves away from 0.1Hz the change in PSD between the incident and transmitted spectrum reduce.

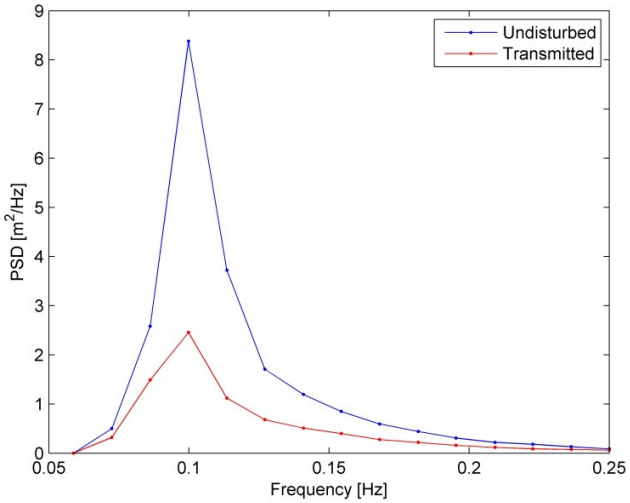

Fig. 3 Frequency dependent power spectral density for the pre and post instillation wave spectrum.

Spatial Distance around a Flat Domain

The spatial disturbance around the array was presented in terms of percentage energy change. This uses the summed spectral moments for all frequency components for an energy proportionate wave height. The wave amplitude is then used to calculate energy and the percentage change in energy is then deduced. The results can split into 2 regions, the device up-wave, where wave-device reflections are dominant and the device down-wave, where transmitted effects are dominant.

Care was taken to remove unphysical artefacts resulting from domain sidewall reflections. A region, indicated by a box in Fig 4, was kept clear of such reflections using a wave-speed dependent post-processing tool. For each frequency component, the tool calculates a wave speed, and hence a maximum simulation time before sidewall reflections enter the area of interest. This allows the slower (shorter wavelength) waves to fully propagate across the domain.

The up-wave results show a complex interaction with a highly variable change in energy across the domain. There are several large increases in wave energy exceeding 15%. Down wave, the change in percentage energy reduces as the distance increases. The edges of the domain shows a small area, 150m behind the central device, where an energy increase is observed. This is a result of the device wake as it propagates down-wave symmetrically from each device, when these regions meet a large positive change in energy occurs.

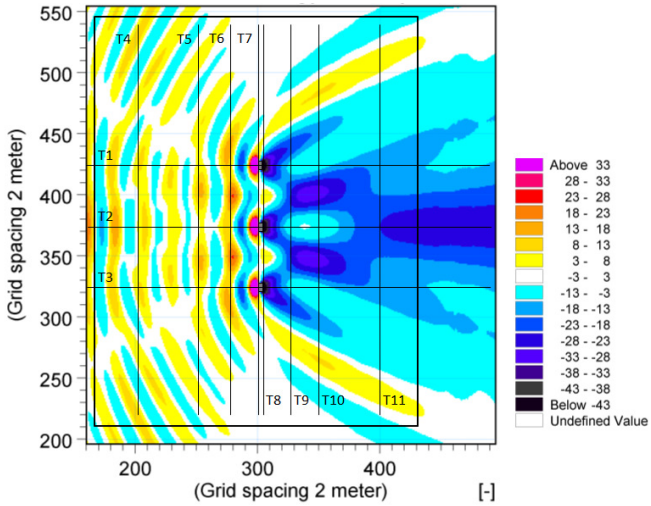

Fig. 4 Percentage change in wave energy for an array of OWSC. Devices locations are at x = 300 and y = 325, 375 and 425 (units in cells).

Several transects were taken across the domain. The locations of these sections are shown in Fig. 4. T1-3 shows the device perpendicular change in wave energy (see Fig. 5). T2 (WEC02) shows the central device, with the side devices transects labelled as T1 (Wec01) and T3 (WEC03). The area immediately around the devices show all transects with identical disturbances. This produces a maximum increase of 96% and a maximum reduction of -59%. As the distance increases reflections and wake interactions cause the central device and the side devices to differ. As the device separation is equal WEC01 and WEC03 have an identical disturbance pattern. The up-wave results of the array shows a reducing modulation in disturbance; at 150m scatter waves from the other devices cause an area of increased energy. The down-wave data separates at 30m, where a peak increase in energy change occurs at 80m behind the device, this is almost equal to the undisturbed energy for the central device. As the distance increases the phase relation changes and the energy reduces. The side devices show a second peak at 320m behind the device.

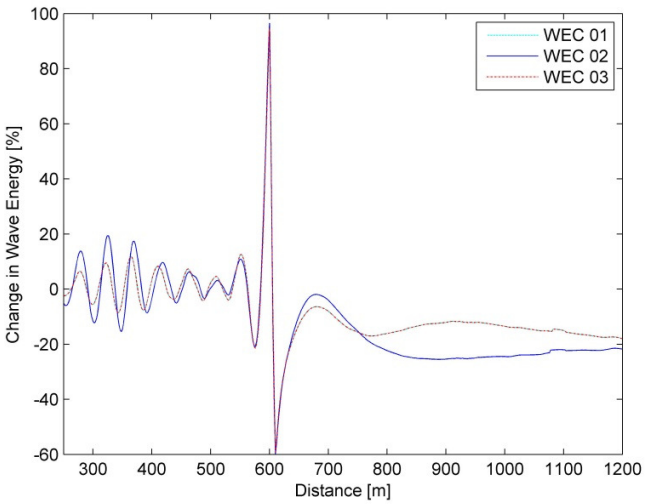

Fig. 5 Percentage change in wave energy from a small array of OWSC on a flat domain for T1-3.

The up-wave results show the devices located at x = 650m, 750m and 850m. Directly in front of each device a large narrow peak is observed, as the distances increases the magnitude severely lessens and the peaks broaden. The complex up-wave energy disturbance further indicates the high spatial variance, where very small correlations between transects can be observed. The 50m and 100m transects are both located near a peak location, the larger distance from the 100m transect shows a much broader spread in disturbance resulting in a low magnitude peak. As the distance increases to 200m the transect shows a large variation at either end, it is this disturbance that if not carefully monitored results in severe sidewall reflections.

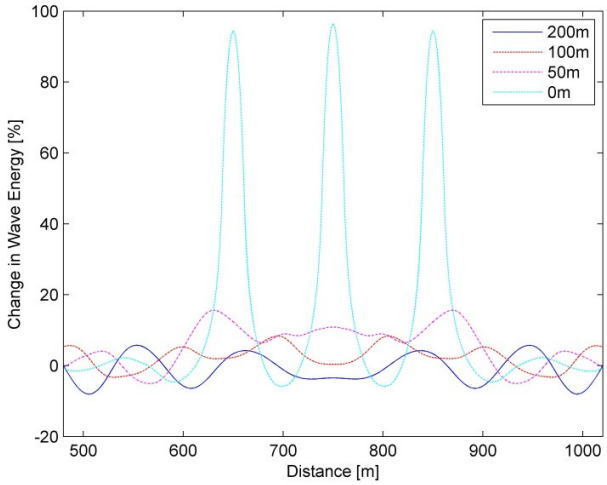

Fig. 6 Up-wave percentage change in wave energy for T4 (200m), T5 (100m), T6 (50m) and T7 (0m) transects.

The down-wave transects show the device locations clearly indicated by the maximum percentage change in the 0m transects (see Fig. 7). The 0m transect experiences a large narrow absorption behind each device, in between which a slight increases in energy is observed. As the distance increases the magnitude of the energy change reduces and the wake distribution spreads. The 50m and the 100m transect crosses in front and behind the main increase in energy change. This results in a minimal energy change behind the devices. The individual device disturbances decrease as the down-wave distance increases, this is illustrated in the 200m transects, where a broad almost U-shaped curve is shown.

The flat domain test demonstrates the application of the frequency dependant absorption. The analysis of the device spectrum shows the presences of the peak reflection and transmission occurring at the peak power capture of the device. The device transects provides large amounts of data on the individual device disturbance interactions. This shows regions of large positive and negative energy changes with several hundred metres of the array.

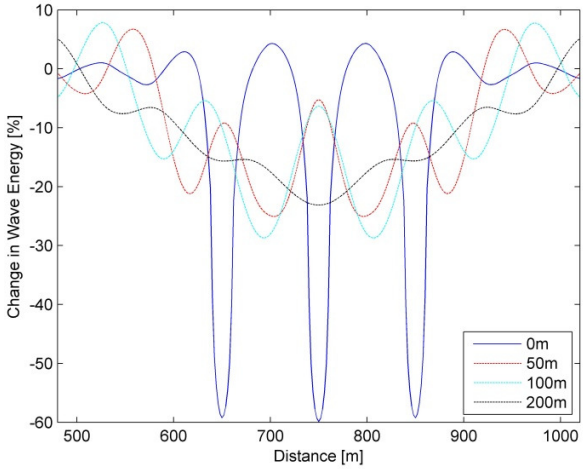

Fig. 7 Down-wave percentage change in wave energy for T8 (0m), T9 (50m), T10 (100m) and T11 (200m).

Spatial Distance around a Uniform Sloped Domain

To test the effects of a uniform bathymetry gradient the previous flat domain was substituted for a uniform sloped domain. The gradient of the slopes tested were selected to be 1:20, 1:50 and 1:100. This provides a steep domain with enough space to include a fully functioning sponge layer behind the array, and a shallow gradient that will provides a slow change in bathymetry. The device location was positioned at the same depth of 10m for each test case. The device spacing was reduced to 50m for the slope simulations. The domain width was increased allowing the expansion of the area of analysis.

The spatial results shown in Fig. 8 have a similar pattern to that of the flat domain. As the device spacing is reduced the combined disturbance values have increased providing a higher spatial energy variance. The steep domain provides a limited area of down-wave analysis. An increased shoreline variation that is dependent on the slope angle is shown between the 1:20 and 1:50 results. The central device transect (Fig. 9) shows a section of device disturbances, with the up-wave useful domain extent shown at 400m. The shoreline position is indicated for the 1:20, 1:50, 1:100 slope gradient at 750m, 1100m and

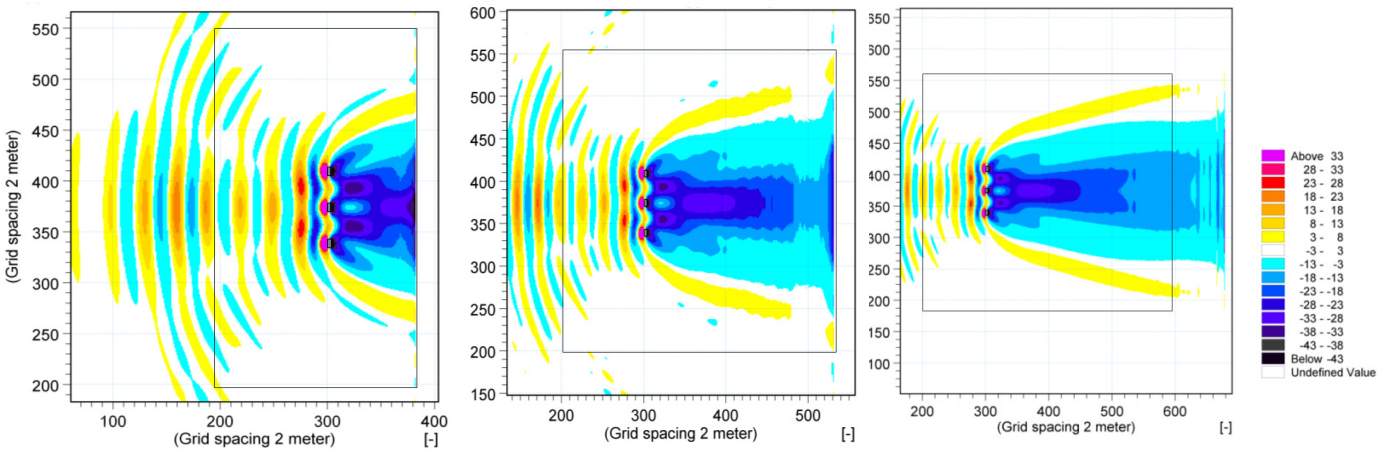

(a) (b) (c)

Fig. 8 Percentage change in wave energy for (a) 1:20, (b) 1:50 and (c) 1:100 domain slope.

1350m respectively, where the device is located at 600m. The up-wave near device disturbance is shown to be identical between tests. As the initial peak begins to oscillate a small increase in disturbance is shown at the peaks and troughs. When the distance in front of the device increases, a slight difference between the wavelengths of the disturbance oscillations can be seen. This is also shown with 1:50 test when the disturbance wavelength is much closer to that of the 1:100 results. The down-wave results exhibit identical disturbances directly behind the array. As the distance increases, combined wake effects produce a peak, the magnitude of which is shown to be slightly larger for the steeper gradient tests. Beyond this a similar disturbance level is observed for all tests. The very nearshore data (depths = 2-3m) are not presented in Fig. 9 as they are located within the end sponge layer and therefore are subject to varying levels of dissipation.

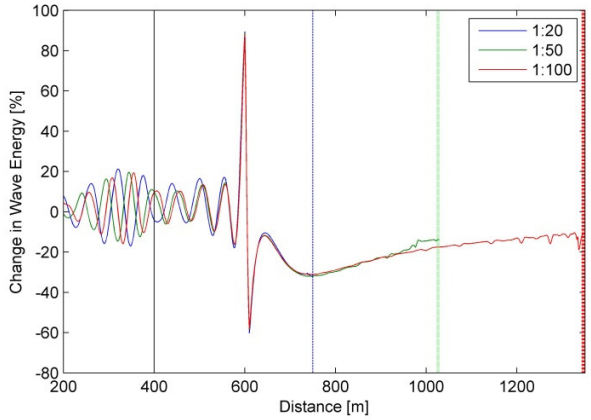

Fig. 9 T2 transects for domain slopes 1:20, 1:50 and 1:100.

These results suggests that the change in slope angle causes has little influence on the near device disturbance, However, as the distance away from the devices increases the steeper gradient domain results in higher peak values. In addition the location of the reflected up-wave peak disturbances is shown to be highly affected. This indicates that the domain gradient plays an important role in the position and the magnitude of the mid-field wave-device disturbances.

CONCLUSONS

This study has demonstrated the method of implementing a frequency dependent WEC simulation within the MIKE21 Boussinesq wave model. With the use of experimental frequency distributed power capture a series of nearshore OWSCs was simulated. The immediate device data shows a peak reflection coefficient of over 0.11 at the peak frequency. An absorption of 5.9m^2/Hz was observed immediately behind a device. The spatial results indicate a complex reflection pattern that causes varying degrees of wave disturbance over short distances. The down-wave results show a general reduction to the change in energy as the distance behind the devices increases. As wake effects interact with these disturbances causing regions of increased energy resulting in a neutral energy change behind the device.

Sloped gradient tests revealed that an increased domain angle caused large changes in the spatial up-wave disturbances, where the steeper slope showed an increase in peak disturbance. The down-wave results reveal a reduced dependency on slope angle; however, wake interaction provided a noticeably larger disturbance for the steep domain. Interestingly, these findings demonstrate that bathymetric slope has an important role on reflected wave-device interaction but only limited effects on the down-wave results.

In recent years, Boussinesq models have often been adopted as a promising pragmatic approach to the challenging problem of incorporating the effects of WECs in wave simulations. This study provides an important refinement to the existing methodology, by developing a mechanism to incorporate frequency-dependent absorption. The next challenge for such models is an explicit treatment of waves radiated from devices. While the effect of radiation will be minimal on the mid-field region of interest in this study, it will be more important in the near-field, and could be simulated using an additional WGL. However, as with most other models, there are restrictions on the availability of phase information for device emitted radiation, which will be strongly dependent on the design, configuration and tuning of the device. In addition, validation of this modelling technique using experimental data would be highly desirable.

ACKNOWLEDGEMENTS

The author wishes to thank the European Regional Development Fund and the TeraWatt EPSRC Grant Ref: EP/J010170/1 project for funding

and software licenses. Addition thanks are conveyed to the marine energy research group at Lews Castle College, UHI and in particular Ruairi Maciver for his input on the analysis of the simulation data.

REFERENCES

Angelelli, E. & Zanuttigh, B. (2012). "A Farm of Wave Activated Bodies for Coastal Protection Purposes", *Proceedings of 33rd International Conference on Coastal Engineering*.

Angelelli, E., Zanuttigh, B. & Kofoed, J.P. (2012). "Numerical modelling of the hydrodynamics around the farm of Wave Activated Bodies", *Proceedings of the 4th International Conference on Ocean Energy* .

Beels, C., Troch, P., De Visch, K., Kofoed, J.P. & De Backer, G. (2010). "Application of the time-dependent mild-slope equations for the simulation of wake effects in the lee of a farm of Wave Dragon wave energy converters", *Renewable Energy,* 35, (8), 1644-1661.

Clabby, D., A. Henry, M. Folley & T. Whittaker (2012). "The effect of the spectral distribution of wave energy on the performance of a bottom hinged flap type wave energy converter", *Procedding of the 31st International Conference on Ocean, Offshore and Arctic Enginerring*.

DHI (2012). "MIKE 21 Spectral Wave Model – Scientific Documentation", [Online],.

Folley, M., Babarit, A., Child, B., Forehand, D., O'Boyle, L., Silverthorne, K., Spinneken, J., Stratigaki, V. & Troch, P. (2012). "A Review of Numerical Modelling of Wave Energy Converter Arrays", *Proceddings of the 31st Internatioal Conference on Ocean, Offshore and Artic Engineering,*.

Goda, Y. (1985). *Random Seas and Design of Maritime Structures,* University of Tokyo Press.

Goda, Y. & Suzuki, Y. (1976). "Estimation of Incident and Reflective Waves in Random Wave Experiments", *Coastal Engineering Proceedings,* 1, 15.

Greenwood, C.E., Venugopal, V., Christie, D., Morrison, J. & Vögler, A. (2013). "Wave modelling for potentail wave energy sites around the Outer Hebrides.", *32th International Conference on Ocean, Offshore and Arctic Engineering*.

Madsen, P.A. & Sorensen, O.R. (1992). "A New Form of Boussinesq Equation with Improved Linear Dispersion Characteristics , Part 2: A Slowly-varying Bathymetry", *Coastal Engineering,*18, 183.

Smith, H.C.M., Pearce, C. & Millar, D.L. (2012). "Further analysis of change in nearshore wave climate due to an offshore wavefarm: An enhanced case study for the Wave Hub site", *Renewable Energy,* 40 (1), 51.

Torch P., C. Beels, J. De Rouck & G. De Backer (2010). "Wake effects behind a farm of wave energy converters for irregular long-crested and short crested waves", *Proceedings of the 32nd International conference of Ocean Eneginerring*.

Venugopal, V., Bryden, I.G. & Wallace, A.R. (2010). "On the interactions of waves with an array of open chambered structures: Applications to wave energy converters", *Proccedings of the 29th International conference on Ocean, Offshore and Arctic Enginerring*.

Venugopal, V. & Smith, G.H. (2007). "Wave climate investigation for an array of wave power devices", *Proceedings of the 7th European Wave and Tidal Energy Conference, Porto, Portugal,*.